Organic Geochemistry 124 (2018) 77–87

Contents lists available at ScienceDirect

Organic Geochemistry

journal homepage: www.elsevier.com/locate/orggeochem

Influence of land use on distribution of soil *n*-alkane δD and brGDGTs along an altitudinal transect in Ethiopia: Implications for (paleo) environmental studies

Andrea Jaeschke [a,*], Janet Rethemeyer [a], Michael Lappé [a], Stefan Schouten [b,c], Pascal Boeckx [d], Enno Schefuß [e]

[a] Institute of Geology and Mineralogy, University of Cologne, Germany
[b] NIOZ Royal Netherlands Institute for Sea Research, Department of Marine Microbiology and Biogeochemistry, and Utrecht University, Den Burg, Texel, The Netherlands
[c] Department of Earth Sciences, Faculty of Geosciences, Utrecht University, The Netherlands
[d] Isotope Bioscience Laboratory - ISOFYS, Faculty of Bioscience Engineering, Ghent University, Belgium
[e] MARUM - Center for Marine Environmental Sciences, University of Bremen, Germany

ARTICLE INFO

Article history:
Received 15 June 2017
Received in revised form 18 April 2018
Accepted 13 June 2018
Available online 15 June 2018

Keywords:
brGDGTs
n-alkanes
δD
$\delta^{13}C$
Altitude
Land use
Ethiopia

ABSTRACT

The combined use of plant wax *n*-alkane δD values and branched glycerol dialkyl glycerol tetraether lipid (brGDGT) distributions provides a novel approach for paleoaltitude reconstruction. Studies from East Africa revealed, however, inconsistent results between the proxy estimates and altitudinal parameters. Here, we explore these proxies in soils of different land use (forest, cropland and pasture) along an altitudinal transect in the Jimma zone of the southwest Ethiopian highlands to better understand environmental and plant-specific factors controlling the isotopic composition and distribution of *n*-alkanes and brGDGTs. The hydrogen isotope composition of individual *n*-alkanes does not unambiguously reflect the altitude effect on precipitation δD, but seems largely influenced by the specific land use. Only forest soil-derived *n*-C_{27} and *n*-C_{29} alkane δD values exhibit a significant linear relationship with altitude (r −0.87, $p < 0.05$), likely reflecting the most stable ecosystem. The resulting lapse rate of −17‰/1000 m is comparable with that of local precipitation in the southwest Ethiopian highlands. In addition, the linear correlation of the average chain length (ACL) and $\delta^{13}C$ values of forest soil *n*-alkanes suggests a physiological adaptation of the specific plant type waxes to altitude-induced environmental changes in the study area. The distribution of brGDGTs also reveals a significant linear correlation with altitude (r −0.97, $p < 0.01$), reflecting the decrease in temperature with higher elevation, independent of land use. In addition, brGDGT-based mean annual air temperature (MAT) estimates of 19.5–14.0 °C and temperature lapse rate of −6 °C/1000 m are in good agreement with direct measurements in the Jimma zone. In contrast to previous studies from East Africa, our results show that both soil *n*-alkane δD values and brGDGT-based MAT distributions track present day altitude effects on local environmental gradients in the southwest Ethiopian highlands.

1. Introduction

In recent years, several new organic proxies have been established to reconstruct changes in marine and terrestrial paleoenvironments. The hydrogen stable isotopic composition (δD) of higher plant wax components (long-chain *n*-alkanes) appears to be a sensitive tracer for reconstructing variation in terrestrial hydrological conditions (Sessions et al., 1999; Schefuß et al., 2005; Rao et al., 2009; Sachse et al., 2012). Plants incorporate the hydrogen isotope composition of source water, and the δD values of the plant wax lipids reflect mainly the isotopic composition of precipitation (e.g. Sachse et al., 2012). However, secondary factors such as evapotranspiration of soil water and leaf water, plant life-form (i.e. tree, shrub, grass) and carbon fixation pathways may also affect the isotopic composition of leaf wax compounds (Smith and Freeman, 2006; Liu and Yang, 2008; Feakins and Sessions, 2010; Kahmen et al., 2013; Gao et al., 2015). The δD value of precipitation in turn is dependent on altitude, i.e. rainfall δD values become successively more depleted with increasing elevation because of rain-out of the heavy isotopologues ('altitude effect'; Dansgaard, 1964). Because of this effect, plant wax δD values have been suggested as

* Corresponding author.
E-mail address: andrea.jaeschke@uni-koeln.de (A. Jaeschke).

https://doi.org/10.1016/j.orggeochem.2018.06.006
0146-6380/

a valuable tool for tracking past elevation change (e.g. Jia et al., 2008; Peterse et al., 2009; Polissar et al., 2009; Bai et al., 2011; Luo et al., 2011; Ernst et al., 2013; Nieto-Moreno et al., 2016). Additional valuable information about vegetation structure and photosynthetic pathway (C_3 vs. C_4) can be obtained by analysing the average chain length (ACL) and stable carbon isotope signature ($\delta^{13}C$) of *n*-alkanes (e.g. Bi et al., 2005; Smith and Freeman, 2006; Feakins and Sessions, 2010; Hoffmann et al., 2013; Tipple and Pagani, 2013; Bush and McInerney, 2015). Both ACL and *n*-alkane $\delta^{13}C$ values have been shown to be sensitive to environmental conditions (temperature, rainfall, relative humidity) and are used as proxies for continental vegetation and climate change (e.g. Schefuß et al., 2003, 2005; Wei and Jia, 2009; Jia et al., 2008; Vogts et al., 2012; Hoffmann et al., 2013; Bush and McInerney, 2015).

Another recently developed molecular proxy for environmental conditions is based on branched glycerol dialkyl glycerol tetraether lipids (brGDGTs; Sinninghe Damsté et al., 2000). These compounds are ubiquitous in soils, lakes and coastal marine sediments, and are presumably produced mainly by anaerobic soil bacteria (e.g. Weijers et al., 2007; Sinninghe Damsté et al., 2011). Empirical studies indicate that the distribution of brGDGTs in soils is controlled mainly by mean annual air temperature (MAT) and soil pH, and can be expressed using the methylation of branched tetraethers (MBT) and the cyclisation of branched tetraethers (CBT) indices. These proxies, or adaptations therefrom, can thus be used to reconstruct soil pH and continental temperature in different geological archives (Weijers et al., 2007; Peterse et al., 2012; De Jonge et al., 2014; Russell et al., 2017). Studies of soil and lake sediments along altitudinal transects in mountain ranges in East Africa, Southeast Asia and the South Central Andes indicate that variation in brGDGT distributions is related to changes in both temperature and altitude, thereby holding promise as viable paleoelevation and paleotemperature proxies (Sinninghe Damsté et al., 2008; Peterse et al., 2009; Tierney et al., 2010; Ernst et al., 2013; Liu et al., 2013; Coffinet et al., 2014, 2017; Nieto-Moreno et al., 2016). However, these studies also reveal caveats in the temperature-altitude relationship of soil-derived brGDGTs, i.e. offsets between measured and calculated MAT. Moreover, potential in-situ production of brGDGTs in lakes or rivers may bias MAT reconstructions in lacustrine environments (Sinninghe Damsté et al., 2009; Tierney et al., 2010; Loomis et al., 2011; Russell et al., 2017). In most of the altitudinal transects studied, a considerable degree of uncertainty in the relationships between the molecular proxies and altitude is apparent (Sinninghe Damsté et al., 2008; Jia et al., 2008; Peterse et al., 2009; Luo et al., 2011; Loomis et al., 2011; Ernst et al., 2013; Coffinet et al., 2014, 2017; Deng et al., 2017). While studies from Mt. Kilimanjaro, Mt. Kenya and Mt. Rungwe in East Africa show that brGDGT-based temperature estimates are consistent with observational temperature values, no clear altitudinal trend is observed for δD values of plant waxes (nC_{29}-nC_{33}, Peterse et al., 2009; nC_{27}-nC_{31}, Coffinet et al., 2017). The lack of a pronounced altitude effect reported in these studies may be caused by local changes in relative humidity or vegetation along elevation transects (Peterse et al., 2009; Zech et al., 2015; Coffinet et al., 2017).

We present here distributions, and stable hydrogen and carbon isotope composition of plant wax *n*-alkanes, as well as brGDGT-based MAT and pH estimates along an elevation gradient from 1769 m to 2650 m above sea level (a.s.l.) in the southwest Ethiopian highlands (Jimma zone). The aim was to gain insight into the applicability of the paleoenvironmental proxies in the region, which is largely impacted by agricultural activity replacing the natural vegetation. The proxies were specifically evaluated for soils of different land use (forest, cropland and pasture) to better understand environmental and plant-specific factors controlling the isotopic composition and distribution of *n*-alkanes and brGDGTs, and likely bias the interpretation for (paleo)altitude studies.

2. Material and methods

2.1. Site description and sampling

The study area is in the Gilgel Gibe catchment in the Jimma zone of the Ethiopian highlands (N7°40′, E36°50′) ca. 260 km southwest of Addis Ababa (Fig. 1). The zone has an area of 18,415 km^2 and an altitudinal range from ca. 1600 to 2700 m (a.s.l.). The MAT and precipitation recorded by two weather stations in the sampling area at Dedo (2100 m a.s.l.) and Jimma (1700 m a.s.l.) are 16.9 °C and 1962 mm and 19.2 °C and 1492 mm, respectively (Fig. 2; http://climate-data.org). Minimum rainfall of the catchment is encountered in the low fluvial plains at 1600 m a.s.l. but is in general never below 1000 mm/yr. Rainfall is restricted to the main rainy season from June to September, sourced by southwesterlies and westerlies, and a shorter rainy period in March-April, associated with the southeastern monsoon (Levin et al., 2009, and references therein).

The reddish to dark brown soils in the area are of volcanic origin, developed from highly weathered basaltic rock material (Deguefu, 1968). The dominant soil type is nitisol (FAO, 2007) characterized by a relatively low pH (< 6; Murphy, 1968; Elias, 2017). The soils are depleted in nutrients due to intensive cultivation, removal of harvest residues and limited availability of mineral fertilizers (Girmay et al., 2008; Takala et al., 2016; Elias, 2017). Soils at higher altitude (sites I-II; Fig. 1; Table 1) are less intensively used than the lower sites III-VI, mainly due to colder temperature and steep slopes of the terrain. At sites I-II, 70–80% of the terrain is used as grazing land (fallow) vs. ca. 10% at sites III-VI. Crops grown on the arable soils include maize, teff, barley, sorghum and cowpea. Mainly eucalyptus is grown at the forest patches as part of the rotation scheme (A. Nebiyu, personal communication).

A total of 54 soil samples was taken at six altitudes from 2650 m to 1769 m a.s.l. (sites I-VI; Fig. 1b) in September 2008. The sampling sites along this toposequence were selected on the basis of different land use as cropland, pasture and forest plantation (Table 1). After removal of the litter layer, ca 0.5 l subsamples (3 replicates for each land use) were taken with a shovel from the 0–15 cm topsoil layer and transferred to glass jars. The samples were thoroughly mixed and air-dried directly upon return to the lab at Jimma University. Samples were sieved through 2 mm mesh and ground with a ball mill.

2.2. Bulk soil analysis and lipid extraction

Total carbon (TC) and total nitrogen (TN) content of 20 mg aliquots were determined using an elemental analyser. For pH analysis, 10 g dry soil were mixed with 25 ml deionised water and shaken in sealed containers for 24 h according to Ryan et al. (2001). The soil pH was measured in the supernatant of the soil-water suspension using a pH meter (PHM62 standard pH meter, radiometer, Denmark).

Dry samples (ca. 24–30 g) were extracted using accelerated solvent extraction (ASE 200, Dionex) with dichloromethane (DCM):MeOH (9:1, v/v). Squalane was added as an internal standard prior to extraction. Each extract was dried using a rotary evaporator and separated into apolar and polar fractions by way of elution with hexane:DCM (9:1, v/v) and DCM:MeOH (1:1, v/v), respectively, over an Al_2O_3 column (active basic, 0.063–0.200 mm, 70–230 mesh ASTM). The apolar fraction was separated into saturated and unsaturated compounds over a small column of silicagel (+230 mesh) impregnated with $AgNO_3$ (ca. 10% w/w) and DCM and EtOAc,

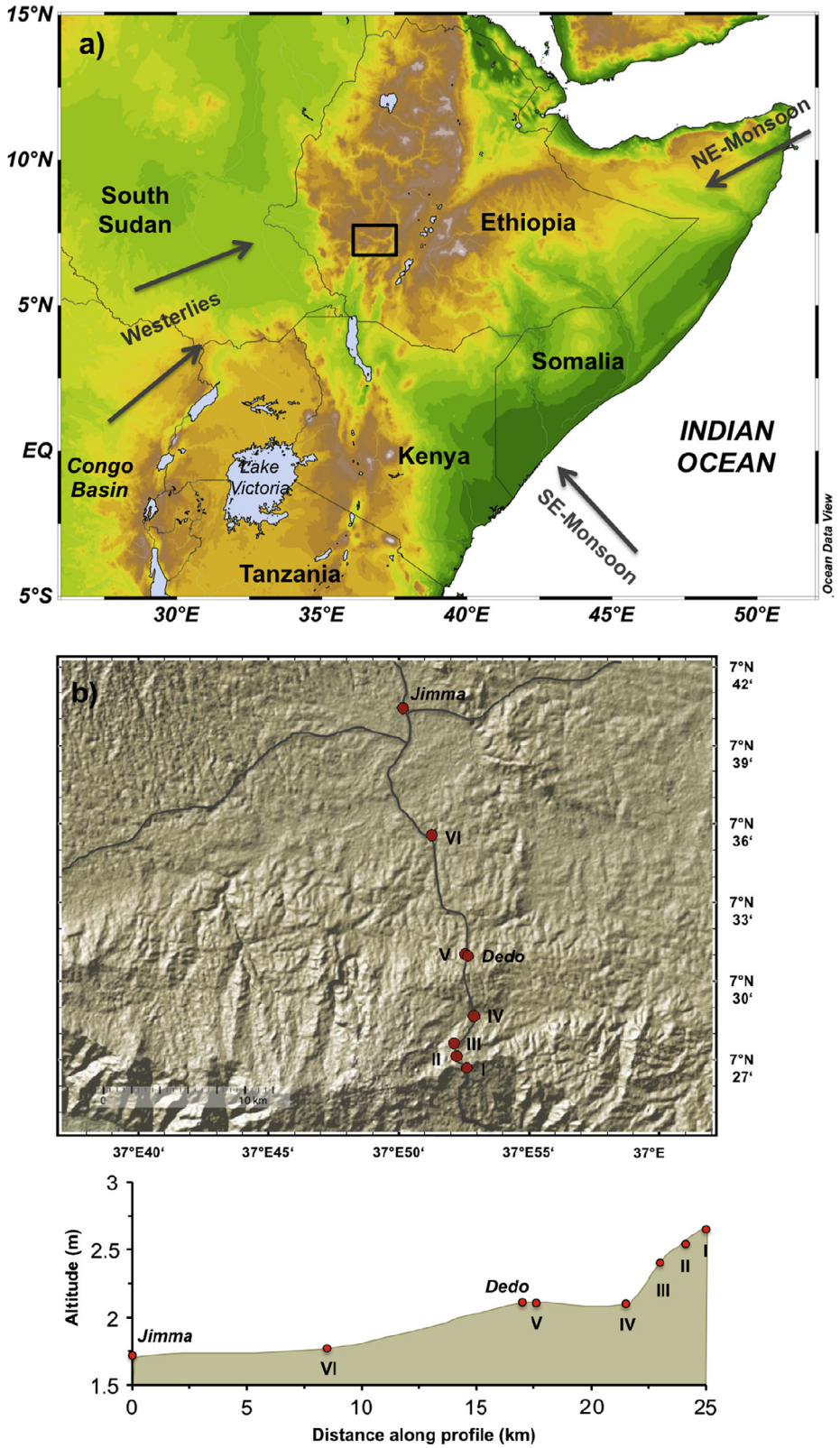

Fig. 1. (a) Topographic map of East Africa. Black rectangle shows study area (Jimma zone) in the SW-Ethiopian highlands. Arrows indicate moisture transport controlled by westerly/southwesterly winds and southeast monsoon (Somali Jet). The northeast monsoon brings predominantly dry air during winter; (b) Topographic map of study area with investigated sites and altitudinal profile along transect.

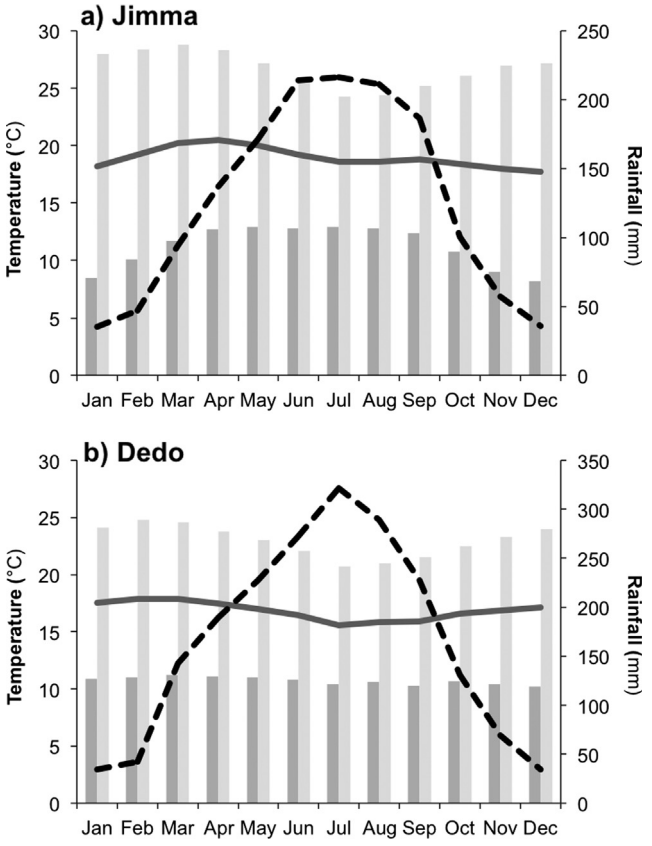

Fig. 2. Mean monthly air temperature (gray line) and rainfall (dashed black line) recorded in (a) Jimma and (b) Dedo, averaged over several decades (http://climate-data.org). Bars indicate minimum (dark gray) and maximum (light gray) monthly temperature.

respectively. The polar fraction, containing the tetraether lipids, was dissolved in hexane:isopropanol (99:1, v/v) and filtered through a 0.45 μm PTFE syringe filter.

2.3. Soil n-alkane $\delta^{13}C$ and δD analysis

n-Alkanes were analysed using gas chromatography with flame ionization detection (GC-FID; HP 5890) and a DB-5MS column (50 m × 0.2 mm, film thickness: 0.33 μm). He was the carrier gas. The oven was programmed from 40 °C to 140 °C at 10 °C/min, and then at 3 °C/min to 320 °C (held 44 min). Assignment of *n*-alkanes was via comparison with an external *n*-alkane standard. Based on repeated analyses of the external standard, the precision of quantification was estimated at ca. 5%.

The carbon preference index (CPI; Bray and Evans, 1961) was calculated using the abundances of odd- and even-numbered *n*-alkane chains from C_{27} to C_{33}:

$$CPI_{27-33} = 0.5 \times \left(\frac{nC_{27} + nC_{29} + nC_{31} + nC_{33}}{nC_{26} + nC_{28} + nC_{30} + nC_{32}} + \frac{nC_{27} + nC_{29} + nC_{31} + nC_{33}}{nC_{28} + nC_{30} + nC_{32} + nC_{34}}\right)$$

The average chain length (ACL) was calculated as follows:

$$ACL_{27-33} = \frac{27 \times nC_{27} + 29 \times nC_{29} + 31 \times nC_{31} + 33 \times nC_{33}}{nC_{27} + nC_{29} + nC_{31} + nC_{33}}$$

Compound-specific stable carbon isotope ($\delta^{13}C$) analysis of long chain *n*-alkanes was accomplished using a Trace GC instrument equipped with a 30 m × 0.25 mm column (Restek Rxi-5 ms, film thickness: 0.25 μm) coupled via a GC/C III interface to a Finnigan MAT 252 mass spectrometer. He was the carrier gas. The fractions were injected via a PTV injector at 40 °C and then transferred to the GC column. The GC oven was programmed from 60 °C (3 min hold) to 150 °C at 20 °C/min, and then at 4 °C/min to 320 °C (held 10 min). Quantitative conversion of eluting compounds to CO_2 was conducted in a ceramic tube filled with Ni wires at 1000 °C using a trickle flow of O_2. CO_2 of known isotope composition was used as reference gas and $\delta^{13}C$ values are reported in ‰ relative to Vienna Peedee Belemnite (VPDB). Only selected samples were analysed for $\delta^{13}C$ values. These were run in duplicate. Repeated analysis of an external *n*-alkane standard yielded long term accuracy and precision of <0.1 and 0.3‰, respectively.

Compound-specific hydrogen isotope (δD) composition of long chain *n*-alkanes was determined with a Trace GC instrument coupled via a pyrolysis reactor to a ThermoFisher Scientific MAT 253 mass spectrometer. The GC instrument was equipped with a 30 m × 0.25 mm column (Restek Rxi-5 ms, film thickness: 0.25 μm) and He was the carrier gas. The fractions were injected via a PTV injector at 40 °C and then transferred to the GC column. The GC temperature program was 60 °C (2 min) to 200 °C at 30 °C/min

Table 1
Site information, surface soil properties, absolute and relative amounts of most abundant long chain *n*-alkanes together with CPI and ACL in soils of different land use along a toposequence in the Jimma zone (SW-Ethiopia).

Site	Lat (°N)	Long (°E)	Altitude (m)	Land use	TOC (%)	C/N	Total wax[a] (μg/g)	*n*-C_{27} (%)	*n*-C_{29} (%)	*n*-C_{31} (%)	*n*-C_{33} (%)	CPI[b]	ACL[c]
I	7.4452	36.8768	2650	Cropland	5.4	9.7	7.9	13	27	30	17	6.3	29.7
				Grassland	7.9	11.9	5.9	14	28	28	16	6.4	29.5
				Forest	4.3	9.3	5.8	15	31	25	14	6.1	29.4
II	7.4527	36.8704	2545	Cropland	3.6	9.1	2.8	14	23	30	18	6.8	29.7
				Grassland	4.2	9.8	1.8	14	22	29	19	5.9	29.8
				Forest	4.7	9.6	5.4	16	24	27	16	6.9	29.4
III	7.4609	36.8687	2402	Cropland	3.1	9.5	2.4	15	23	28	17	5.9	29.5
				Grassland	2.9	9.2	2.7	16	20	28	18	5.5	29.4
				Forest	3.0	9.4	3.9	16	28	24	15	6.9	29.5
IV	7.4782	36.8814	2099	Cropland	2.8	9.1	1.7	16	24	29	17	5.7	29.5
				Grassland	3.2	9.3	2.3	15	21	27	20	5.7	29.6
				Forest	3.8	9.3	3.3	16	28	24	16	7.1	29.2
V	7.5176	36.8758	2109	Cropland	2.7	9.5	1.6	16	24	26	17	6.1	29.4
				Grassland	2.7	10.1	2.4	18	22	24	17	5.8	29.3
				Forest	3.6	9.5	3.9	17	26	24	15	7.0	29.2
VI	7.593	36.8544	1769	Cropland	2.8	11.2	2.1	14	22	25	17	6.0	29.6
				Grassland	3.0	10.6	2.3	16	19	19	16	5.0	29.1
				Forest	3.7	10.5	4.6	14	23	21	17	6.0	29.0

[a] Sum of odd C_{25}-C_{35} *n*-alkanes.
[b] $CPI_{27-33} = 0.5 \times \Sigma(C_{27}\text{-}C_{33})/(C_{26}\text{-}C_{32}) + 0.5 \times \Sigma(C_{27}\text{-}C_{33})/(C_{28}\text{-}C_{34})$.
[c] $ACL_{27-33} = \Sigma(i \times Xi)/\Sigma Xi$, where X is abundance and i range from *n*-C_{27} to *n*-C_{33}.

and then at 4 °C/min to 320 °C (held 12.3 min). H_2 was the reference gas and δD values are given in ‰ relative to Vienna Standard Mean Ocean Water (VSMOW). The H_3 factor ranged between 7.58 and 7.74 over the measuring period (7.63 ± 0.05). All samples were analysed in triplicate. An external *n*-alkane standard was analysed repeatedly in between samples and yielded accuracy and precision of <1 and 2‰, respectively.

The isotopic fractionation between plant wax and precipitation ($\varepsilon_{wax\text{-}p}$) was calculated as follows:

$$\varepsilon_{wax-p} = 1000 \times \frac{(\delta Dwax + 1000)}{(\delta Dp + 1000)} - 1$$

The online isotopes in precipitation calculator (OIPC) was used to estimate modern mean annual and monthly hydrogen isotopic composition of precipitation (δD_p) based on the site location and elevation (Bowen and Revenaugh, 2003; Bowen, 2016). A limitation of the model is the uneven spatial distribution of stations with isotopic data for precipitation (Bowen and Revenaugh, 2003). The modeled δD_p composition is generally in good agreement with measured δD values of meteoric water from Ethiopia, which are unusually high vs. other high altitude settings in Africa (Levin et al., 2009). In the southwestern Ethiopian highlands, the main rainy season (June-September) is fed by a combination of westerly and southwesterly winds, whereas the shorter rain period in spring (March/April) is associated with the southeast monsoon. The southeasterly winds are normally deflected by the southern Ethiopian highlands and so may not reach the study area. The westerlies/southwesterlies, which bring transpired (recycled) moisture from terrestrial sources in South Sudan and the Congo Basin, have been proposed to be likely responsible for the anomalously high isotope values of rainfall in Ethiopia (Levin et al., 2009).

2.4. GDGT analysis

GDGTs were analysed using high performance liquid chromatography/atmospheric pressure chemical ionization-mass spectrometry (HPLC-APCI-MS) with an Agilent 1100 chromatograph connected to an MSD SL mass detector according to Schouten et al. (2007). Separation of crenarchaeol and brGDGTs was achieved with an Alltech Prevail Cyano column (150 mm × 2.1 mm; 3 μm). The compounds were eluted with 90% hexane/10% hexane:isopropanol (9:1, v/v) for 5 min (0.2 ml/min), and then with a linear gradient to 16% hexane:isopropanol (9:1, v/v) for 34 min. The injection volume was 10 μl. GDGTs were detected using single ion monitoring (SIM) of $[M+H]^+$ ions (dwell time 234 ms). GDGTs were quantified via integration of peak areas.

Samples were additionally re-run with the new HPLC-APCI-MS method established by Hopmans et al. (2016), which enables separation of the 5- and 6-methyl brGDGT isomers that co-elute on a traditional Prevail Cyano Column.

The CBT (cyclisation ratio of branched tetraethers; Weijers et al., 2007) and MBT′ (methylation index of branched tetraethers; Peterse et al., 2012) indices were calculated according to the following equations:

$$CBT = -\log\left(\frac{[Ib + IIb + IIb']}{[Ia + IIa + IIa']}\right)$$

$$MBT' = \frac{(Ia + Ib + Ic)}{(Ia + Ib + Ic + IIa + IIb + IIc + IIIa + IIa' + IIb' + IIc' + IIIa')}$$

Soil pH and MAT′ values were calculated using the global calibration sets by Peterse et al. (2012):

$$pH = 7.9 - 1.97 \times CBT$$

$$MAT' = 0.81 - 5.65 \times CBT + 31.0 \times MBT'$$

In addition, the recently introduced MAT_{mr} index, based on multiple linear regressions of brGDGT fractional abundances correlating with MAT, was calculated after De Jonge et al. (2014):

$$MAT_{mr} = 7.17 + 17.1 \times [Ia] + 25.9 \times [Ib] + 34.4 \times [Ic] - 28.6 \times [IIa]$$

The newly defined CBT′ index and pH were calculated as follows (De Jonge et al., 2014):

$$CBT' = \log\left(\frac{[Ic + IIa' + IIb' + IIc' + IIIa' + IIIb' + IIIc']}{[Ia + IIa + IIIa]}\right)$$

$$pH = 7.15 + 1.59 \times CBT'$$

The BIT (branched vs. isoprenoid tetraether) index was calculated according to Hopmans et al. (2004):

$$BIT = \frac{(Ia + IIa + IIIa)}{(Ia + IIa + IIIa + Crenarchaeol)}$$

The roman numerals correspond to 5-methyl brGDGTs with 4–6 methyl branches (I-III) containing 0–3 cyclopentane moieties (a-c). The 6-methyl brGDGTs are indicated by a prime symbol after the roman numerals for the corresponding 5-methyl isomers (De Jonge et al., 2014).

3. Results and discussion

3.1. Variation in vegetation parameters across a land use profile in southwest Ethiopia

Long-chain *n*-alkanes detected in soils along the altitudinal transect in the Jimma zone ranged from *n*-C_{25} to *n*-C_{35}, with *n*-C_{29} or *n*-C_{31} most abundant (Table 1). Total *n*-alkane concentration ranged from 1.6 to 7.9 μg/g, with the highest concentration generally in forest soils (Table 1). A strong odd/even distribution, reflected in high CPI values between 5.0 and 7.1 (Table 1), is typical for a predominant contribution from higher plant wax (Eglinton and Hamilton, 1967). This is also indicated by high TOC content (2.7–7.9%) and C/N ratio values of 9.1–11.9 (Table 1), in the range reported for agricultural soils in the Ethiopian highlands (Elias, 2017). ACL ranged between 29.0 and 29.8 (Table 1). ACL is suggested to change with plant type and/or environmental conditions, i.e. temperature and hydroclimate (Maffei, 1996; Schefuß et al., 2003; Jia et al., 2008; Hoffmann et al., 2013; Tipple and Pagani, 2013; Bush and McInerney, 2015). The average ACL of 29.3 in the forest soils is at the upper end reported for eucalyptus leaves (26.8–29.3; Hoffmann et al., 2013; Kahmen et al., 2013). In our study, this may relate to the fact that soil OM reflects an integrated *n*-alkane signal from the overall vegetation, with a likely contribution of extended (i.e. *n*-C_{31} and *n*-C_{33}) from understory grass. Hoffmann et al. (2013) observed highest ACL at sites characterized by highest annual precipitation of 1600 mm/yr, in good agreement with our sites where mean precipitation is similarly high and ranges between 1492 mm/yr (Jimma) and 1962 mm/yr (Dedo; Fig. 2). Moreover, our forest soil ACL values linearly increase with altitude (r 0.91, $p = 0.012$; Fig. 3). A similar trend was observed at Mt. Gongga, China and ACL was suggested to relate to vegetation type variation along the slope transect (Bai et al., 2011). We cannot explain the observed altitudinal increase in ACL with major vegetation change in our forest soils as eucalyptus is the prevailing plant type at all sites. Instead, changes in temperature or humidity along the study transect might largely control concentration and

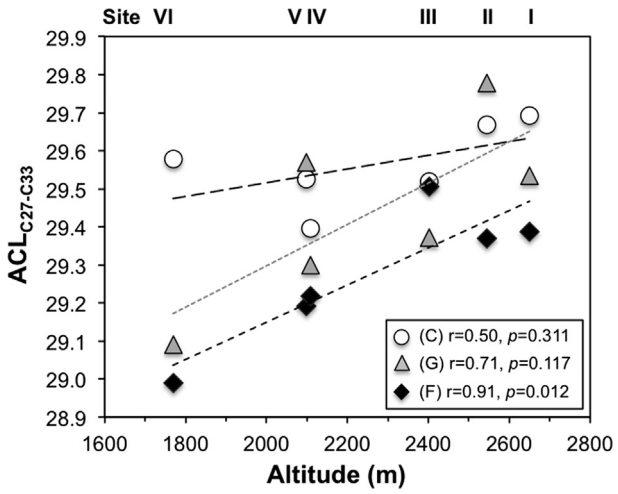

Fig. 3. Variation in ACL of soil *n*-alkanes from different land use with altitude in the Jimma zone. C, cropland; G, grassland; F, forest.

chain length distributions of *n*-alkanes (Hoffmann et al., 2013; Bush and McInerney, 2015). The relationship was less pronounced in samples from grassland and especially cropland (Fig. 3). A diverse mixture of C_3 and C_4 grasses, cereals and legumes growing at the grassland and cropland sites (Section 2.1) might explain the ambiguous signals.

To discriminate between C_3 and C_4 plant contributions, we analysed $\delta^{13}C$ values of individual *n*-alkanes from forest, grassland and cropland soils. The values for forest soil-derived *n*-alkanes varied between -29.0 ± 0.2‰ at site VI and -35.7 ± 0.2‰ at site I (Fig. 4; Table S1 in Supplementary material), indicating a dominance of C_3 plants (Collister et al., 1994; Still et al., 2003; Castañeda et al, 2009) and were largely consistent with those of *n*-alkanes from tropical and subtropical African woodland C_3 dicots (Vogts et al., 2009). At site I (2650 m a.s.l.) *n*-alkanes extracted from grassland soils exhibited comparable $\delta^{13}C$ values ranging from -31.6 ± 0.2‰ to -34.6 ± 0.3‰ (Fig. 4; Table S1 in Supplementary material), indicating a predominance of C_3 grasses. In contrast, $\delta^{13}C$ values of *n*-alkanes derived from cropland sites III-VI displayed more positive values ranging from -23.9 ± 0.1‰ to -29.1 ± 0.1‰ (Fig. 4; Table S1 in Supplementary material), suggesting a contribution from C_4 plants. This obvious difference may be explained by the diverging intensity of agricultural use at the different sites, and $\delta^{13}C$ values are comparable with those reported for topsoil of cultivated land in the Ethiopian highlands (Eshetu and Högberg, 2000; Girmay et al., 2008). Site V is in close proximity to the city of Dedo, a densely populated area. The arable land is used for continuous cultivation of C_4 crops (e.g. maize, sorghum, teff) and C_3 crops (e.g. barley) in rotation with fallowing (A. Nebiyu, personal communication). It is thus likely that this caused the bias towards less negative $\delta^{13}C$ values in the grassland soils.

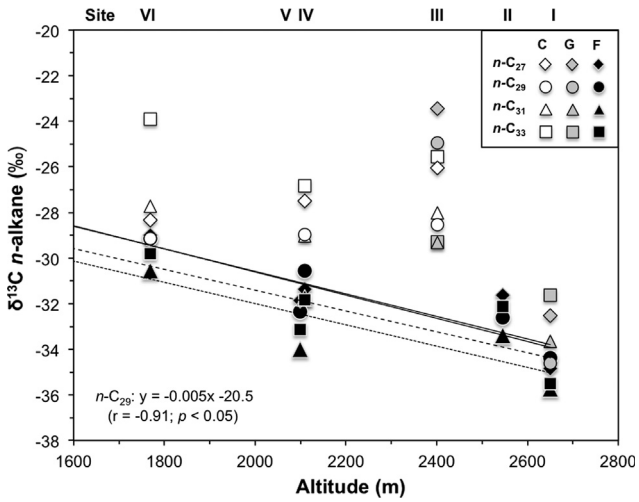

Fig. 4. Altitudinal trend in $\delta^{13}C$ values of individual soil *n*-alkanes from forest (F, black symbols), grassland (G, gray symbols), and cropland (C, white symbols).

The $\delta^{13}C$ values of forest soil *n*-alkanes displayed a systematic trend towards more negative values with altitude (−5‰/1000 m; Fig. 4). On a global scale, C_3 plant $\delta^{13}C$ values are generally thought to increase with altitude, caused by higher water-use efficiency with decreasing temperature and lower atmospheric partial pressure of CO_2 at higher altitude (e.g. Körner et al., 1988, 1991). However, the global pattern of plant $\delta^{13}C$ values (−0.9‰ to 2.7‰/1000 m) was established from humid areas (Körner et al., 1988). In more arid regions, drought stress may overtake other factors in controlling changes in plant $\delta^{13}C$ value with elevation (Van de Water et al., 2002; Song et al., 2008; Wei and Jia, 2009). These opposing trends in carbon isotope discrimination with altitude were documented for elevation transects up to 2800 m on the Tibetan Plateau (Song et al., 2008; Wei and Jia, 2009), and largely agree with our observations for a similar elevation range and precipitation amount. Drought stress is in general not thought to be a major issue in the area of the Gilgel Gibe catchment. However, besides a suggested precipitation threshold value required for plant $\delta^{13}C$ response (Wei and Jia, 2009), edaphic factors such as nutrient status and low soil water content as a result of intense agriculture could be potential environmental drivers of the observed variation in our *n*-alkane $\delta^{13}C$ values across the gradient (Warren et al., 2001). In the Jimma zone, both forest soil *n*-alkane $\delta^{13}C$ values and chain length distribution reveal a distinct altitude effect (Figs. 3 and 4). Moreover, significant correlations between the two parameters (Fig. S1 in Supplementary material) may reflect the common dependence of both on environmental gradients, such as growing season temperature and humidity (Bush and McInerney, 2015).

3.2. Relationship between soil n-alkane δD values and elevation

Compound-specific δD values of the most abundant wax *n*-alkanes (*n*-C_{27} to *n*-C_{33}) ranged between -125 ± 2‰ and -148 ± 1‰ (Table 2), and isotopic variation within individual *n*-alkanes from a specific vegetation type, i.e. grassland, cropland, forest, was in general relatively small (2–15‰). It is commonly assumed that precipitation δD (δD_p) is the primary control on plant wax δD values (e.g. Sachse et al., 2012). Previous studies used either the weighted mean δD of the most common *n*-alkanes (i.e. *n*-C_{27-33}) or a predominant *n*-alkane, which was suggested to reflect the effect of altitude on the δD signal (Jia et al., 2008; Ernst et al., 2013; Nieto-Moreno et al., 2016). Following previous approaches, we first evaluated the potential of the most abundant *n*-alkanes (Table 1) as a recorder of δD_p, and thus altitude in the Jimma zone. Correlation of *n*-alkane δD with modeled annual and seasonal δD_p (Bowen and Revenaugh, 2003; Bowen, 2016) revealed δD variation among individual homologues, which cannot be related to the specific type of land use or environmental variables (Table S2 in Supplementary material). Significant linear relationships were only observed between forest soil *n*-C_{27} and *n*-C_{29} alkane δD and mean annual δD_p (r 0.87 and 0.84, respectively), while δD values of the extended (*n*-C_{31} and *n*-C_{33}) alkanes from forest soil showed no relationship with δD_p (Table S2 in Supplementary material). Moreover, soil *n*-alkanes from grassland and cropland showed no correlation with δD_p, so other factors must be primarily controlling their isotopic signature, such as life-form or photosynthetic pathway (Sachse et al.,

Table 2
δD values of soil *n*-alkanes and modeled precipitation δD values along a toposequence in the Jimma zone (SW-Ethiopia).

Site	Altitude (m)	Land use	δDp[a] (‰)	δD[b] *n*-C_{27} (‰)	δD *n*-C_{29} (‰)	δD *n*-C_{31} (‰)	δD *n*-C_{33} (‰)
I	2650	Cropland	−13	−130 ± 6	−130 ± 7	−131 ± 7	−137 ± 8
		Grassland		−137 ± 3	−133 ± 1	−130 ± 2	−136 ± 1
		Forest		−144 ± 8	−138 ± 2	−129 ± 1	−130 ± 2
II	2545	Cropland	−11	−136 ± 2	−132 ± 6	−133 ± 6	−139 ± 3
		Grassland		−144 ± 5	−142 ± 2	−140 ± 1	−146 ± 2
		Forest		−148 ± 1	−138 ± 1	−135 ± 1	−139 ± 1
III	2402	Cropland	−9	−126 ± 5	−130 ± 6	−130 ± 0	−131 ± 3
		Grassland		−130 ± 3	−128 ± 2	−132 ± 2	−132 ± 3
		Forest		−132 ± 8	−130 ± 3	−129 ± 3	−127 ± 3
IV	2099	Cropland	−5	−129 ± 4	−127 ± 6	−127 ± 5	−134 ± 1
		Grassland		−135 ± 7	−131 ± 2	−132 ± 4	−133 ± 3
		Forest		−131 ± 4	−132 ± 3	−130 ± 3	−130 ± 3
V	2109	Cropland	−5	−132 ± 5	−130 ± 6	−128 ± 10	−129 ± 9
		Grassland		−130 ± 8	−132 ± 6	−134 ± 6	−136 ± 7
		Forest		−130 ± 2	−127 ± 2	−125 ± 1	−129 ± 4
VI	1769	Cropland	0	−129 ± 2	−134 ± 2	−131 ± 4	−133 ± 7
		Grassland		−136 ± 4	−132 ± 2	−134 ± 5	−143 ± 8
		Forest		−125 ± 2	−127 ± 2	−133 ± 2	−139 ± 9

[a] Modeled mean annual precipitation δD for different altitudes in Jimma zone according to Bowen and Revenaugh (2003) and Bowen (2016).
[b] Analytical error of triplicate measurements given.

2012). C_4 plants tend to build longer chains and show more positive $\delta^{13}C$ values than C_3 plants (e.g. Collister et al., 1994), the latter also apparent from our $\delta^{13}C$ values (Section 3.1). In addition, C_4 grasses show greater hydrogen isotope fractionation against source water than C_3 trees and shrubs but lower than C_3 grasses (e.g. Sachse et al., 2012; Smith and Freeman, 2006). Our study area is characterized largely by anthropogenic influence through intense cultivation of varying crop types (i.e. cereal-legume rotation) and pasture, which may have caused the distorted δD signal by way of variable mixtures of C_3 and C_4 plant-derived wax components. Eucalyptus plantations are often also part of the rotation scheme but normally grow on steeper slopes where crop cultivation is difficult, thereby generally remaining constant for several years (A. Nebiyu, personal communication). It is therefore plausible that the eucalyptus forest soils preserve the most stable signal. The strong correlation (Table S2 in Supplementary material) of the *n*-C_{27} alkane with δD_p seems surprising, as it is not one of the predominant *n*-alkanes in the samples (Table 1), but is in accord with its dominance in woody plants (Maffei, 1996; Hoffmann et al., 2013). The extended *n*-C_{31} and *n*-C_{33} alkanes must therefore at least partly derive from other plants growing between the eucalyptus trees, most likely C_3 grasses as indicated by the $\delta^{13}C$ values (Section 3.1). We suggest using the weighted mean $\delta D_{C27+C29}$ in the Jimma zone as the most appropriate recorder of the altitude effect on precipitation (r −0.87, $p < 0.05$; Fig. 5). This is in contrast to other altitudinal transects from East Africa, which showed no clear trend for δD_{wax} (e.g. Peterse et al., 2009; Zech et al., 2015; Coffinet et al., 2017) and may indicate regionally different controls (i.e. change in vegetation and/or relative humidity) on the link between altitude and soil *n*-alkane δD. The isotopic fractionation between annual precipitation and C_{27+29} *n*-alkanes ($\varepsilon_{wax\text{-}p}$) from the forest soils showed little variation with altitude ($\varepsilon_{wax\text{-}p}$ −123‰ to −134‰) and is quite similar to the average apparent fractionation reported for leaf wax *n*-alkanes from trees (e.g. Sachse et al., 2012). Our $\varepsilon_{wax\text{-}p}$ values are between those for rainforest locations in Cameroon (up to −154‰; Garcin et al., 2012) and those found in a marine sediment transect off southwest Africa (avg. −109‰; Vogts et al., 2016). These $\varepsilon_{wax\text{-}p}$ values are in the range of observed climate-specific $\varepsilon_{wax\text{-}p}$ values for tropical zones with a distinct dry season (Luo et al., 2011).

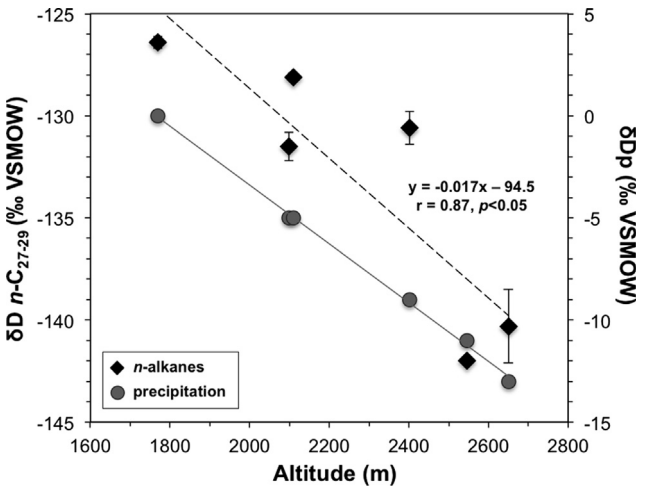

Fig. 5. δD values of forest soil *n*-alkanes (weighted mean *n*-C_{27+29}) and modeled annual precipitation (Bowen and Revenaugh, 2003) along an elevation transect in the Jimma zone.

The δD_{C27+29} lapse rate of −17 ± 2‰/1000 m based on the forest soil *n*-alkanes falls into the range of reported δD_p values of −10 to −40‰/1000 m in mountain areas (Araguás-Araguás et al., 2000), and conforms to the annual δD_p lapse rate of −14‰/1000 m in the Jimma zone (Fig. 5). Our δD_{wax} lapse rate is also comparable with those recorded for Mt. Gongga, China (−18‰/1000 m; Jia et al., 2008), the Meghalaya Plateau, India (−20‰/1000 m; Ernst et al., 2013), and the South Central Andes (−16‰/1000 m; Nieto-Moreno et al., 2016), although these areas experience fundamentally different hydrological conditions than East Africa.

3.3. Temperature and pH estimation based on brGDGTs

GDGT analysis showed typical soil distributions, i.e. dominated by brGDGTs, with only small amounts of crenarchaeol, resulting in high BIT index values of 0.91–0.99 (Table 3), typical for most soils (Schouten et al., 2013). Distinct changes in the brGDGT distribution with altitude were observed, and reflected in the CBT and MBT′ indices. CBT varied between 0.88 and 1.43 corresponding, using the global soil correlation of Peterse et al. (2012), to estimated pH of 5.1–6.2 (Table 3). These values are close to the average soil pH of 5.5 reported for nitisols in the area (Murphy, 1968; Elias, 2017). The revised CBT′ index of De Jonge et al. (2014) yielded similar pH values between 5.3 and 6.5 (Table 3 in Supplementary material). The poor relationship between CBT and measured soil

Table 3
Soil pH, GDGT-based index values together with MAT′ estimates and CBT-derived pH according to Peterse et al. (2012) for soils of different land use along a toposequence in the Jimma zone (SW-Ethiopia).

Site	Altitude (m)	Land use	pH meas.	BIT	MBT′[a]	CBT[a]	MAT′ (°C)	pH calc.
I	2650	Cropland	5.7	0.94	0.64 ± 0.05	0.91 ± 0.28	15.4 ± 0.3	6.1 ± 0.7
		Grassland	5.3	0.97	0.64 ± 0.01	1.05 ± 0.21	14.6 ± 0.7	5.8 ± 0.5
		Forest	5.5	0.97	0.57 ± 0.05	0.88 ± 0.41	13.7 ± 1.2	6.2 ± 1.1
II	2545	Cropland	5.6	0.96	0.66 ± 0.02	1.33 ± 0.12	13.9 ± 1.2	5.3 ± 0.3
		Grassland	5.4	0.99	0.72 ± 0.01	1.43 ± 0.17	15.0 ± 1.2	5.1 ± 0.5
		Forest	5.4	0.98	0.62 ± 0.02	1.22 ± 0.42	13.0 ± 1.7	5.5 ± 1.1
III	2402	Cropland	5.6	0.95	0.70 ± 0.03	1.27 ± 0.25	15.4 ± 0.5	5.4 ± 0.7
		Grassland	5.5	0.98	0.76 ± 0.05	1.35 ± 0.28	16.7 ± 0.2	5.3 ± 0.7
		Forest	5.8	0.98	0.67 ± 0.05	1.08 ± 0.37	15.4 ± 0.6	5.8 ± 1.0
IV	2099	Cropland	5.8	0.93	0.79 ± 0.03	1.20 ± 0.28	18.4 ± 2.0	5.5 ± 0.7
		Grassland	5.7	0.98	0.81 ± 0.01	1.38 ± 0.17	18.2 ± 1.0	5.2 ± 0.4
		Forest	5.3	0.97	0.72 ± 0.05	1.25 ± 0.50	16.2 ± 1.4	5.4 ± 1.3
V	2109	Cropland	5.7	0.92	0.77 ± 0.03	1.33 ± 0.24	17.1 ± 1.0	5.3 ± 0.6
		Grassland	5.6	0.95	0.76 ± 0.01	1.40 ± 0.18	16.6 ± 0.8	5.1 ± 0.5
		Forest	5.6	0.97	0.73 ± 0.03	1.10 ± 0.07	17.4 ± 0.7	5.7 ± 0.2
VI	1769	Cropland	5.8	0.91	0.83 ± 0.02	1.32 ± 0.12	19.1 ± 1.1	5.3 ± 0.3
		Grassland	5.8	0.98	0.86 ± 0.03	1.43 ± 0.13	19.6 ± 0.2	5.1 ± 0.3
		Forest	5.8	0.94	0.82 ± 0.08	1.13 ± 0.27	19.7 ± 1.0	5.7 ± 0.7

[a] Analytical error of triplicate measurements given.

pH (r −0.38, p 0.005; Fig. S2 in Supplementary material) may be due to the narrow pH range of 5.3–5.8 in our samples (Table 3). This may be related to the input of organic and mineral fertilizers in the study area (Sasakawa Global 2000, 2004), which can significantly alter soil pH at the sites of intense agricultural use (i.e. cropland and grassland). Moreover, soil acidification due to Fe leaching and organic acids from the eucalyptus litter has been observed in the Jimma zone (Carrasco-Letelier et al., 2003). Despite this, our data (Fig. 6a) fit well with the global calibration set of Peterse et al. (2012), indicating that the distribution of brGDGTs still mirrors the pH of agricultural soils subjected to external influences (Fig. 6b).

The distribution of brGDGTs has been shown to correlate globally with pH and MAT over a range of conditions (e.g. Weijers et al., 2007; Peterse et al., 2012; Naafs et al., 2017). Recent studies also observed linear altitudinal gradients of MAT estimates along mountain ranges in East Africa, Southeast Asia, and the South-Central Andes, thereby demonstrating the potential of brGDGTs as a viable (paleo)elevation proxy (Sinninghe Damsté et al., 2008; Peterse et al., 2009; Ernst et al., 2013; Liu et al., 2013; Coffinet et al., 2014, 2017; Nieto-Moreno et al., 2016). However, a degree of uncertainty in absolute MAT was suggested to relate to a potential seasonal bias in MBT-CBT derived temperature estimates. The bias may be caused by a distinct season of optimum growth of the brGDGT-producing bacteria or local environmental factors, such as water availability (Loomis et al., 2011; Peterse et al., 2012; Menges et al., 2014; Deng et al., 2017). The recently developed MAT_{mr} proxy of De Jonge et al. (2014) further allows reconstruction of temperature independent of pH and was proposed to improve the accuracy of MAT reconstruction for relatively arid regions (mean annual precipitation MAP < 1000 mm). Our MAT_{mr}-based temperature values linearly decreased from 20.9 °C at 1769 m to 12.5 °C at 2650 m (Fig. 7; Table S3 in Supplementary material). The calculated MAT_{mr} (mean value of forest, cropland and grassland soils) showed a strong correlation with altitude (r −0.98, $p < 0.01$; Fig. 7). The resulting lapse rate of −8.6 ± 1.3 °C/1000 m is, however, higher than that based on weather station data (−5.6 °C/1000 m) but values are well within the reported calibration error (De Jonge et al., 2014). MAT estimates based on the MBT′/CBT calibration of Peterse et al. (2012) ranged from 19.7 °C at 1769 m to 13.0 °C at 2650 m (Table 3), and mean MAT values showed a similar strong relationship with altitude (r −0.97, $p < 0.01$; Fig. 7). A closer inspection of the MAT estimates from soils of different land use showed almost identical lapse rate for

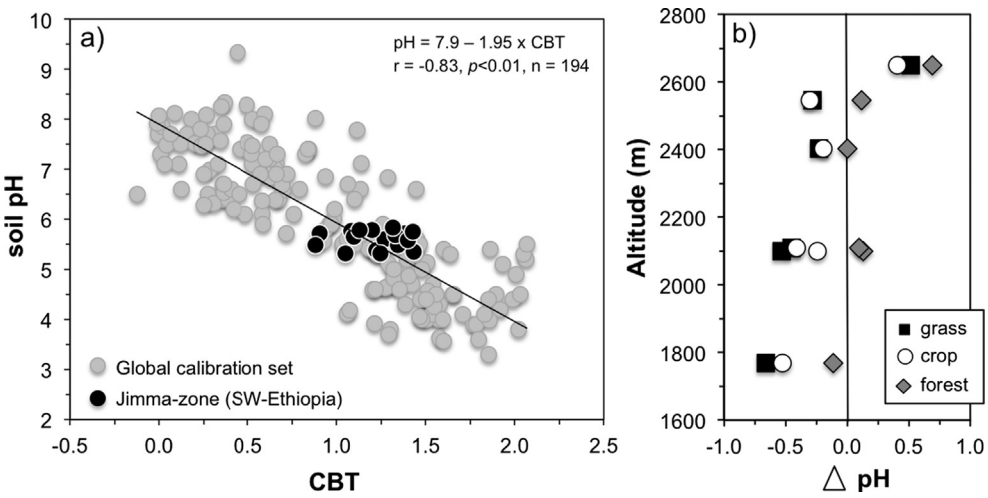

Fig. 6. (a) Relationship between CBT and measured pH for soils of different land use along a toposequence in the Jimma zone (SW-Ethiopia) and the global soil compilation (Peterse et al., 2012); (b) offset between measured and calculated pH values for soils of different land use (root mean square error, RMSE: crop 0.4, grass 0.5, forest 0.3).

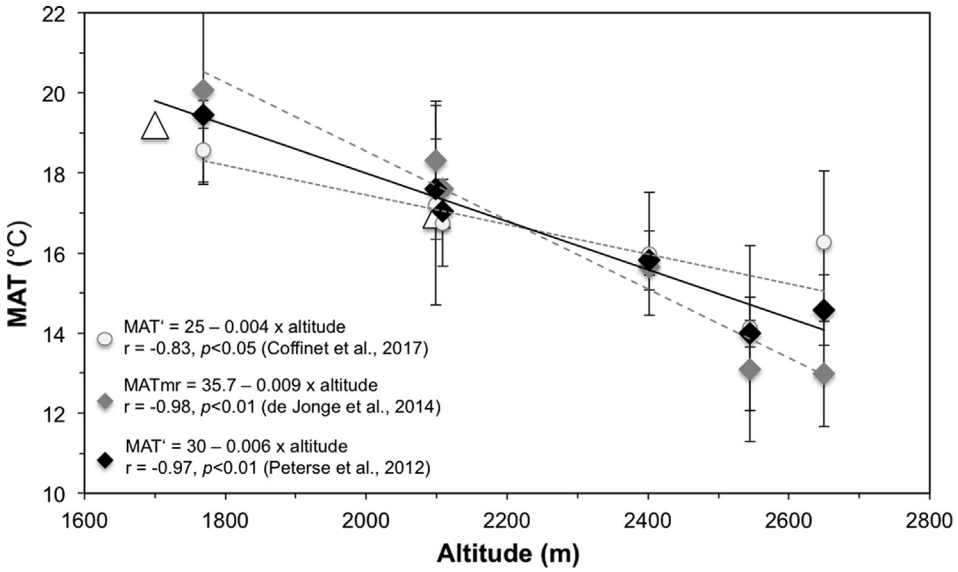

Fig. 7. MBT′/CBT based MAT (black; Peterse et al., 2012) and multiple linear regression-based MATmr (gray; De Jonge et al., 2014) estimates along an elevation transect in the Jimma zone (SW-Ethiopia). MAT estimates based on regional calibration of Coffinet et al. (2017) are indicated as white dots. Values show mean MAT from soils of different land use for each site. White triangles indicate measured MAT from two weather stations in Jimma and Dedo, respectively.

cropland and grassland (−5.5 and −5.4 °C/1000 m, respectively) while it was slightly higher for forest soil (−7.2 °C/1000 m; Fig. S3 in Supplementary material). The resulting mean lapse rate of -6 ± 0.7 °C/1000 m is in good agreement with the observed lapse rate derived from weather stations in the Jimma zone and in Ethiopia (Fazzini et al., 2015). In contrast, the recently proposed regional calibration for reconstructing MAT in East Africa (Coffinet et al., 2017) did not improve our MAT estimates (Fig. 7; Fig. S4 in Supplementary material). Thus, the MBT′-CBT proxy tracks temperature change with altitude in the Jimma zone with a comparable lapse rate to that compiled for East Africa (−5.2 °C/1000 m; Coffinet et al., 2017) and confirms its robustness as a paleoelevation proxy.

4. Conclusions

We assessed the suitability of *n*-alkane distributions, *n*-alkane $\delta^{13}C$ and δD composition, as well as brGDGT distributions in soils of different land use (forest, cropland, grassland) along an elevation transect in the southwest Ethiopian highlands as proxies for paleoenvironmental conditions. Soil-derived *n*-alkane δD values of individual homologs did not unambiguously reflect the altitude effect on precipitation δD, but seemed largely influenced by the specific land use. Only forest soil-derived *n*-C_{27} and *n*-C_{29} alkane δD values exhibited a significant linear relation with altitude (r −0.87, $p < 0.05$), likely because forest reflects the most stable ecosystem. The resulting lapse rate of −17‰/1000 m is comparable with that of local precipitation in the southwest Ethiopian highlands. In addition, the linear correlation of ACL and $\delta^{13}C$ values of forest soil *n*-alkanes with altitude suggests a physiological adaptation of the specific plant type waxes to altitude-induced environmental changes. The GDGT-based proxy seems to be largely unaffected by the different land use in the study area. Temperature estimates based on the MBT′/CBT indices showed a strong relationship with altitude (r −0.97, $p < 0.01$), and a lapse rate of −6 °C/1000 m that is comparable with the observed lapse rate based on weather station data in the Jimma zone. In addition, CBT-based pH estimates largely corresponded to measured soil pH in the study area, even in manipulated soils. Our results show that distributions of brGDGTs and *n*-alkane δD values can be used for paleoclimate reconstruction in East Africa but also emphasize that information on the vegetation structure is required when using *n*-alkane δD as a paleoelevation proxy.

Acknowledgements

We thank N. Jacobs for providing unpublished results from his MSc Thesis. P.B. thanks the VLIROUS IUC project and A. Nebiyu from Jimma University for field assistance and local support. M.L. thanks the DAAD for financial support. E.S. acknowledges funding through the DFG-Research Center/Cluster of Excellence "The Ocean in the Earth System" at MARUM - Center for Marine Environmental Sciences, University of Bremen. S.S. acknowledges funding through the Netherlands Earth System Science Center funded by the Dutch Ministry of Education, Culture and Science. We thank three anonymous reviewers for constructive comments.

Appendix A. Supplementary material

Supplementary data associated with this article can be found, in the online version, at https://doi.org/10.1016/j.orggeochem.2018.06.006.

Associate Editor—**C. Turich**

References

Araguás-Araguás, L., Froehlich, K., Rozanski, K., 2000. Deuterium and oxygen-18 isotope composition of precipitation and atmospheric moisture. Hydrological Processes 14, 1341–1355.
Bai, Y., Fang, X., Gleixner, G., Mügler, I., 2011. Effect of precipitation regime on δD values of soil *n*-alkanes from elevation gradients – implications for the study of paleo-elevation. Organic Geochemistry 42, 838–845.
Bi, X., Sheng, G., Liu, X., Li, C., Fu, J., 2005. Molecular and carbon and hydrogen isotopic composition of n-alkanes in plant leaf waxes. Organic Geochemistry 36, 1405–1417.
Bowen, G.J., Revenaugh, J., 2003. Interpolating the isotopic composition of modern meteoric precipitation. Water Resources Research 39, 1299.
Bowen, G.J., 2016. The Online Isotopes in Precipitation Calculator OIPC, version 2.2, online available at: http://waterisotopes.org, last access: June 2016.
Bray, E.E., Evans, E.D., 1961. Distribution of normal paraffins as a clue to recognition of source beds. Geochimica et Cosmochimica Acta 22, 2–15.
Bush, R.T., McInerney, F.A., 2015. Influence of temperature and C_4 abundance on *n*-alkane chain length distributions across the central USA. Organic Geochemistry 79, 65–73.

Carrasco-Letelier, L., Eguren, G., Castineira, C., Parra, O., Panario, D., 2003. Preliminary study of prairies forested with Eucalyptus sp. at the northwestern Uruguayan soils. Environmental Pollution 127, 49–55.
Castañeda, I.S., Mulitza, S., Schefuß, E., Lopes dos Santos, R., Sinninghe Damsté, J.S., Schouten, S., 2009. Wet phases in the Sahara/Sahel region and human migration patterns in North Africa. Proceedings of the National Academy of Sciences 106, 20159–20163.
Coffinet, S., Huguet, A., Williamson, D., Fosse, C., Derenne, S., 2014. Potential of GDGTs as a temperature proxy along an altitudinal transect at Mount Rungwe (Tanzania). Organic Geochemistry 68, 82–89.
Coffinet, S., Huguet, A., Pedentchouk, N., Bergonzini, L., Omuombo, C., Williamson, D., Anquetil, C., Jones, M., Majule, A., Wagner, T., Derenne, S., 2017. Evaluation of branched GDGTs and leaf wax *n*-alkane δ^2H as (paleo) environmental proxies in East Africa. Geochimica et Cosmochimica Acta 198, 182–193.
Collister, J.W., Rieley, G., Stern, B., Eglinton, G., Fry, B., 1994. Compound-specific δ^{13}C analyses of leaf lipids from plants with differing carbon dioxide metabolisms. Organic Geochemistry 21, 619–627.
Dansgaard, W., 1964. Stable isotopes in precipitation. Tellus 16, 436–468.
Deguefu, D., 1968. Soil fertility studies of Kaffa province. Experimental Station Bulletin No 63, College of Agriculture, Haile Selassie I University, Dire Dawa.
De Jonge, C., Hopmans, E.C., Zell, C.I., Kim, J.H., Schouten, S., Sinninghe Damsté, J.S., 2014. Occurrence and abundance of 6-methyl branched glycerol dialkyl glycerol tetraethers in soils: implications for paleoclimate reconstruction. Geochimica et Cosmochimica Acta 141, 97–112.
Deng, L., Jia, G., Jin, C., Li, S., 2017. Warm season bias of branched GDGT temperature estimates causes underestimation of altitudinal lapse rate. Organic Geochemistry 96, 11–17.
Eglinton, G., Hamilton, R.J., 1967. Leaf epicuticular waxes. Science 156, 1322.
Elias, E., 2017. Characteristics of Nitisol profiles as affected by land use type and slope class in some Ethiopian highlands. Environmental Systems Research 6, 20. https://doi.org/10.1186/s40068-017-0097-2.
Ernst, N., Peterse, F., Breitenbach, S.F.M., Syiemlieh, H.J., Eglinton, T.I., 2013. Biomarkers record environmental changes along altitudinal transects in the wettest place on Earth. Organic Geochemistry 68, 82–89.
Eshetu, Z., Högberg, P., 2000. Reconstruction of forest site history in Ethiopian highlands based on ^{13}C natural abundance of soils. Ambio 29, 83–89.
Fazzini, M., Bsici, C., Billi, P., 2015. The climate of Ethiopia. In: Billi, P. (Ed.), Landscapes and Landforms in Ethiopia, World Geomorphological Landscapes. Springer Science and Business Media Dordrecht http://doi.org/10.1007/978-94-017-8026-1_3.
Feakins, S.J., Sessions, A.L., 2010. Controls on the D/H ratios of plant leaf waxes in an arid ecosystem. Geochimica et Cosmochimica Acta 72, 2128–2141.
Food and Agriculture Organization, 2007. World Reference Base for Soil Resources www.fao.org.
Gao, L., Guimond, J., Thomas, E., Huand, Y., 2015. Major trends in leaf wax abundance, δ2H and δ13C values along leaf venation in five species of C3 plants: physiological and geochemical implications. Organic Geochemistry 78, 144–152.
Garcin, Y.G., Schwab, V.F., Gleixner, G., Kahmen, A., Todou, G., Séné, O., Onana, J.M., Achoundong, G., Sachse, D., 2012. Hydrogen isotope ratios of lacustrine sedimentary *n*-alkanes as proxies of tropical African hydrology: insights from across a calibration transect in Cameroon. Geochimica et Cosmochimica Acta 79, 106–126.
Girmay, G., Singh, B.R., Mitiku, H., Borresen, T., Lal, R., 2008. Carbon stocks in Ethiopian soils in relation to land use and soil management. Land Degradation & Development 19, 351–367.
Hoffmann, B., Kahmen, A., Cernusak, L.A., Arndt, S.K., Sachse, D., 2013. Abundance and distribution of leaf wax *n*-alkanes in leaves of Acacia and Eucalyptus trees along a strong humididty gradient in northern Australia. Organic Geochemistry 62, 62–67.
Hopmans, E.C., Weijers, J.W.H., Schefuß, E., Herfort, L., Sinninghe Damsté, J.S., 2004. A novel proxy for terrestrial organic matter in sediments based on branched and isoprenoid tetraether lipids. Earth and Planetary Science Letters 24, 107–116.
Hopmans, E.C., Schouten, S., Sinninghe Damsté, J.S., 2016. The effect of improved chromatography on GDGT-based palaeoproxies. Organic Geochemistry 93, 1–6.
Jia, G., Wei, K., Chen, F., Peng, P., 2008. Soil *n*-alkane δD vs. altitude gradients along Mount Gongga, China. Geochimica et Cosmochimica Acta 72, 5165–5174.
Kahmen, A., Hoffmann, B., Schefuß, E., Arndt, S.K., Cernusak, L.A., West, J.B., Sachse, D., 2013. Leaf water deuterium enrichment shapes leaf wax *n*-alkane δD values of angiosperm plants II: Observational evidence and global implications. Geochimica et Cosmochimica Acta 111, 50–63.
Körner, C., Farquhar, G.D., Roksandic, Z., 1988. A global survey of carbon isotope discrimination in plants from high altitude. Oecologia 74, 623–632.
Körner, C., Farquhar, G.D., Wong, S.C., 1991. Carbon isotope discrimination by plants follows latitudinal and altitudinal trends. Oecologia 88, 30–40.
Levin, N.E., Zipser, E.J., Cerling, T.E., 2009. Isotopic composition of waters from Ethiopia and Kenya: insights into moisture sources for eastern Africa. Journal of Geophysical Research 114, D23306.
Liu, W., Yang, H., 2008. Multiple controls for the variability of hydrogen isotopic compositions in higher plant *n*-alkanes from modern ecosystems. Global Change Biology 14, 2166–2177.
Liu, W., Wang, H., Zhang, C.L., Liu, Z., He, Y., 2013. Distribution of glycerol dialkyl glycerol tetraether lipids along an altitudinal transect on Mt. Xiangpi, NE Qinghai-Tibetan Plateau, China. Organic Geochemistry 57, 76–83.
Loomis, S.E., Russell, J.M., Sinninghe Damsté, J.S., 2011. Distributions of branched GDGTs in soils and lake sediments from western Uganda: implications for a lacustrine paleothermometer. Organic Geochemistry 42, 739–751.
Luo, P., Peng, P.A., Gleixner, G., Zheng, Z., Pang, Z.H., Ding, Z.L., 2011. Empirical relationship between leaf wax *n*-alkane δD and altitude in the Wuyi, Shennongjia and Tianshan Mountains, China: implications for paleoaltimetry. Earth and Planetary Science Letters 301, 285–296.
Maffei, M., 1996. Chemotaxonomic significance of leaf wax alkanes in the Gramineae. Biochemical Systematics and Ecology 24, 53–64.
Menges, J., Huguet, C., Alcañiz, J.M., Fietz, S., Sachse, D., Rosell-Melé, A., 2014. Influence of water availability in the distributions of branched glycerol dialkyl glycerol tetraethers in soils of the Iberian Peninsula. Biogeosciences 11, 2571–2581.
Murphy, H.F., 1968. A report on the fertility status and some other data on some soils of Ethiopia. Experimental Station Bulletin No. 44, College of Agriculture, Haile Selassie I University, Dire Dawa.
Naafs, B.D.A., Inglis, G.N., Zheng, Y., Amesbury, M.J., Biester, H., Bindler, R., Blewett, J., Burrows, M.A., del Castillo Torres, D., Chambers, F.M., Cohen, A.D., Evershed, R.P., Feakins, S.J., Galka, M., Gallego-Sala, A., Gandois, L., Gray, D.M., Hatcher, P. G., Honorio Coronado, E.N., Hughes, P.D.M., Huguet, A., Könönen, M., Laggoun-Défarge, F., Lähteenoja, O., Lamentowicz, M., Marchant, R., McClymont., E., Pontevedra-Pombal, X., Ponton, C., Pourmand, A., Rizzuti, A.M., Rochefort, L., Schellekens, J., De Vleeschouwer, F., Pancost, R.D., 2017. Introducing global peat-specific temperature and pH calibrations based on brGDGT bacterial lipids. Geochimica et Cosmochimica Acta 208, 285–301.
Nieto-Moreno, V., Rohrmann, A., Van der Meer, M.T.J., Sinninghe Damsté, J.S., Sachse, D., Tofelde, S., Niedermeyer, E.M., Strecker, M.R., Mulch, A., 2016. Elevation-dependent changes in *n*-alkane δD and soil GDGTs across the South-Central Andes. Earth and Planetary Science Letters 453, 234–242.
Peterse, F., van der Meer, M.T.J., Schouten, S., Jia, G., Ossebaar, J., Blokker, J., Sinninghe Damsté, J.S., 2009. Assessment of soil *n*-alkane δD and branched tetraether membrane lipid distributions as tools for paleoelevation reconstruction. Biogeosciences 6, 2799–2807.
Peterse, F., van der Meer, M.T.J., Schouten, S., Weijers, J.W.H., Fierer, N., Kim, J.H., Sinninghe Damsté, J.S., 2012. Revised calibration of the MBT-CBT paleotemperature proxy based on branched tetraether membrane lipids in surface soils. Geochimica et Cosmochimica Acta 96, 215–229.
Polissar, P.J., Freeman, K.H., Rowley, D.B., McInerney, F.A., Currie, B.S., 2009. Paleoaltimetry of the Tibetan Plateau from D/H ratios of lipid biomarkers. Earth and Planetary Science Letters 287, 64–76.
Rao, Z., Zhu, Z., Jia, G., Henderson, A.C.G., Xue, Q., Wang, S., 2009. Compound specific δD values of long chain *n*-alkanes derived from terrestrial higher plants are indicative of the δD of meteoric waters: evidence from surface soils in eastern China. Organic Geochemistry 40, 922–930.
Russell, J.M., Hopmans, E.C., Loomis, S.E., Liang, J., Sinninghe Damsté, J.S., 2017. Distributions of 5- and 6-methyl branched glycerol dialkyl glycerol tetraethers (brGDGTs) in East African lake sediments: effects of temperature, pH, and new lacustrine paleotemperature calibrations. Organic Geochemistry 117, 56–69.
Ryan, J., Estefan, G., Rashid, A., 2001. Soil and Plant Analysis Laboratory Manual. International Center for Agricultural Research in the Dry Areas (ICARDA), Aleppo, Syria, 172 pp.
Sachse, D., Billault, I., Bowen, G.J., Chikaraishi, Y., Dawson, T.E., Feakins, S.E., Freeman, K.H., Magill, C.R., McInerney, F.A., Van der Meer, M.T.J., Polissar, P., Robins, R.J., Sachs, J.P., Schmidt, H.L., Sessions, A.L., White, J.W.C., West, J.B., Kahmen, A., 2012. Molecular paleohydrology: Interpreting the hydrogen-isotopic composition of lipid biomarkers from photosynthesizing organisms. Annual Review of Earth and Planetary Sciences 40, 221–249.
Sasakawa Global 2000, 2004. Optimizing fertiliser use in Ethiopia: Proceedings of the workshop on soil-test calibration study in Hetosa Wereda, Arsi Zone 10/12/2002.
Schefuß, E., Ratmeyer, V., Stuut, J.B.W., Jansen, J.H.F., Sinninghe Damsté, J.S., 2003. Carbon isotope analyses of *n*-alkanes in dust from the lower atmosphere over the central eastern Atlantic. Geochimica et Cosmochimica Acta 67, 1757–1767.
Schefuß, E., Schouten, S., Schneider, R.R., 2005. Climatic controls on central African hydrology during the past 20,000 years. Nature 427, 1003–1006.
Schouten, S., Huguet, C., Hopmans, E.C., Kienhuis, M.V.M., Sinninghe Damsté, J.S., 2007. Analytical methodology for TEX_{86} paleothermometry by high-performance liquid chromatography/atmospheric pressure chemical ionization-mass spectrometry. Analytical Chemistry 79, 2940–2944.
Schouten, S., Hopmans, E.C., Sinninghe Damsté, J.S., 2013. The organic geochemistry of glycerol dialkyl glycerol tetraether lipids: a review. Organic Geochemistry 54, 19–61.
Sessions, A.L., Burgoyne, T.W., Schimmelmann, A., Hayes, J.M., 1999. Fractionation of hydrogen isotopes in lipid biosynthesis. Organic Geochemistry 30, 1193–1200.
Sinninghe Damsté, J.S., Hopmans, E.C., Pancost, R.D., Schouten, S., Geenevasen, J.A.J., 2000. Newly discovered non-isoprenoid glycerol dialkyl glycerol tetraether lipids in sediments. Chemical Communications 1683–1684.
Sinninghe Damsté, J.S., Ossebaar, J., Schouten, S., Verschuren, D., 2008. Altitudinal shifts in the branched tetraether lipid distribution in soil from Mt. Kilimanjaro (Tanzania): implications for the MBT/CBT continental paleothermometer. Organic Geochemistry 39, 1072–1076.
Sinninghe Damsté, J.S., Ossebaar, J., Abbas, B., Schouten, S., Verschuren, D., 2009. Fluxes and distribution of tetraether lipids in an equatorial African lake: constraints on the application of the TEX_{86} paleothermometer and BIT index in lacustrine settings. Geochimica et Cosmochimica Acta 73, 4232–4249.
Sinninghe Damsté, J.S., Rijpstra, W.I.C., Hopmans, E.C., Weijers, J.W.H., Foesel, B.U., Overmann, J., Dedysh, S.N., 2011. 13,16-Dimethyl octacosanedioic acid (iso-diabolic acid): a common membrane-spanning lipid of Acidobacteria subdivisions 1 and 3. Applied and Environmental Microbiology 77, 4147–4154.

Smith, F.A., Freeman, K.H., 2006. Influence of physiology and climate on δD of leaf wax *n*-alkanes from C_3 and C_4 grasses. Geochimica et Cosmochimica Acta 70, 1172–1187.

Song, M.H., Duan, D.Y., Chen, H., Hu, Q.W., Zhang, F., Xu, X.L., Tian, Y.Q., Ouyang, H., Peng, C.H., 2008. Leaf $\delta^{13}C$ reflects ecosystem patterns and responses of alpine plants to the environments on the Tibetan Plateau. Ecography 31, 499–508.

Still, C.J., Berry, J.A., Collatz, G.J., DeFries, R.J., 2003. Global distribution of C_3 and C_4 vegetation: carbon cycle implications. Global Biogeochemical Cycles 17, 1006.

Takala, W., Adugna, T., Tamam, D., 2016. Land use land cover change using Multi Temporal Landsat data in Gilgel Gibe Basin, Ethiopia. International Journal of Science and Technology 5, 309–323.

Tierney, J.E., Russell, J.M., Eggermont, H., Hopmans, E.C., Verschuren, D., Sinninghe Damsté, J.S., 2010. Environmental controls on branched tetraether lipid distributions in tropical East African lake sediments. Geochimica et Cosmochimica Acta 74, 4902–4918.

Tipple, B.J., Pagani, M., 2013. Environmental control on eastern broadleaf forest species' leaf wax distributions and D/H ratios. Geochimica et Cosmochimica Acta 111, 64–77.

Van de Water, P.K., Leavitt, S.W., Betancourt, J.L., 2002. Leaf $\delta^{13}C$ variability with elevation, slope transect, and precipitation in the southwest United States. Oecologia 132, 332–343.

Vogts, A., Moossen, H., Rommerskirchen, F., Rullkötter, J., 2009. Distribution patterns and stable carbon isotopic composition of alkanes and alkan-1-ols from plant waxes of African rain forest and savanna C_3 species. Organic Geochemistry 40, 1037–1054.

Vogts, A., Schefuß, E., Badewien, T., Rullkötter, J., 2012. *n*-Alkane parameters from a deep sea sediment transect off southwest Africa reflect continental vegetation and climate conditions. Organic Geochemistry 47, 109–119.

Vogts, A., Badewien, T., Rullkötter, J., Schefuß, E., 2016. Near-constant apparent hydrogen isotope fractionation between leaf wax *n*-alkanes and precipitation in tropical regions: evidence from a marine sediment transect off SW Africa. Organic Geochemistry 96, 18–27.

Warren, C.R., McGrath, J.F., Adams, M.A., 2001. Water availability and carbon isotope discrimination in conifers. Oecologia 127, 476–486.

Wei, K., Jia, G., 2009. Soil *n*-alkane $\delta^{13}C$ along a mountain slope as an integrator of altitude effect on plant species $\delta^{13}C$. Geophysical Research Letters 36, L11401.

Weijers, J.W.H., Schouten, S., van den Donker, J.C., Hopmans, E.C., Sinninghe Damsté, J.S., 2007. Environmental controls on bacterial tetraether membrane lipid distribution in soils. Geochimica et Cosmochimica Acta 71, 703–713.

Zech, M., Zech, R., Rozanski, K., Gleixner, G., Zech, W., 2015. Do n-alkane biomarkers in soil/sediments reflect the $\delta^{2}H$ isotopic composition of precipitation? A case study from Mt. Kilimanjaro and implications for paleoaltimetry and paleoclimate research. Isotopes in Environmental Health Studies 51, 508–524.